Evidence for Submesoscale Barriers to Horizontal Mixing in the Ocean from Current Measurements and Aerial Photographs

HEZI GILDOR

Weizmann Institute of Science, Rehovot, Israel

ERICK FREDJ

The Jerusalem College of Technology, Jerusalem, Israel

JONAH STEINBUCK AND STEPHEN MONISMITH

Stanford University, Stanford, California

(Manuscript received 8 August 2008, in final form 2 February 2009)

ABSTRACT

Ocean submesoscale (~2–20 km) mixing processes play a major role in ocean dynamics, in physical–biological interactions (e.g., in the dispersion of larvae), and in the dispersion of pollutants. In this paper, horizontal mixing on a scale of a few kilometers is investigated, from observations of surface currents, using highly resolved (300 m) high-frequency radar. These results show the complexity of ocean mixing on scales of a few kilometers and the existence of temporary barriers to mixing that can affect the dispersion of biological materials and pollutants. These barriers are narrow [O(100 m)] and can survive for a few days. The existence of these barriers is supported in simultaneous aerial photographs. The barriers observed here may require a new approach to the way horizontal mixing is parameterized in ocean and climate models.

1. Introduction

Ocean mixing processes span a wide range of spatial and temporal scales, from millimeters to basin-wide and from microseconds to decades and beyond. Numerous recent studies have investigated ocean mixing on mesoscales or larger (d'Ovidio et al. 2004; Lehahn et al. 2007; Waugh et al. 2006) using velocity fields derived from drifters (LaCasce and Ohlmann 2003; Olascoaga et al. 2006), numerical models (d'Ovidio et al. 2004; Orre et al. 2006; Garcia-Olivares et al. 2007), and observations from satellites (Waugh et al. 2006; Lehahn et al. 2007). These studies demonstrate the nonuniform characteristics of mixing and the existence of coherent structures.

Unlike these previous studies, here we concentrate on the submesoscale structure of horizontal mixing. Capet et al. (2008) define the submesoscale regime as having a horizontal scale of O(10 km), less than the first internal Rossby radius, with a vertical scale of O(10 m), and with a time scale of O(1 day). Thomas et al. (2008) use "submesoscale" to refer to vorticity dynamics characterized by a ratio of relative vorticity to planetary vorticity that is O(1). The flow field analyzed in the present study fits both definitions. An example vorticity map normalized by the Coriolis parameter f from 3 February 2006 (one of the days analyzed in detail in section 3) can be seen in Fig. 1.

Submesoscale mixing processes are difficult to observe and quantify. However, it is well recognized that they play a critical role in modulating large-scale circulation (Van haren et al. 2004), ecological functioning and carbon sequestration in surface waters (Williams and Follows 2003), and the dispersion of pollutants (Waugh et al. 2006). Accurate parameterizations of submesoscale mixing processes are critical in simulating and predicting ocean circulation and changes in the climate (Waugh et al. 2006). Because of the limited computer power, present-day ocean and climate models resolve processes

Corresponding author address: Hezi Gildor, Department of Environmental Sciences and Energy Research, Weizmann Institute of Science, Rehovot 76100, Israel.
E-mail: hezi.gildor@weizmann.ac.il

DOI: 10.1175/2009JPO4116.1

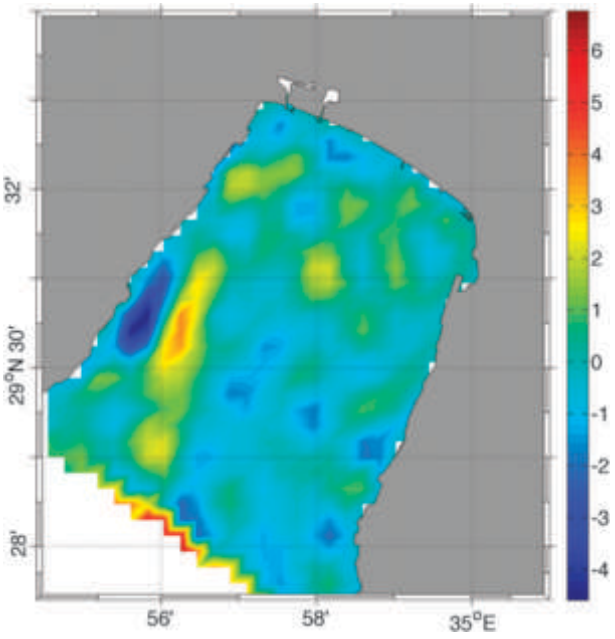

FIG. 1. Relative vorticity normalized by the Coriolis parameter f for the velocity field at 2330 UTC 3 Feb 2006, one of the days analyzed in detail in section 3. This characteristic ratio is $O(1)$ for submesoscale dynamics as defined by Thomas et al. (2008).

on scales down to a few tens of kilometers. The combined effect of subgrid processes, including different types of instabilities and waves, has to be parameterized, and this is typically done using diffusion-like parameterizations, with an ''eddy diffusivity'' that is larger than molecular diffusivity, but which implies similar physical characteristics to that of molecular diffusion. Two implications to using homogeneous (or even just smoothly varying) eddy diffusivity are that first, there are no barriers to mixing and, second, that the average absolute dispersion of particles (i.e., the average displacement of particles from their origins) grows in proportion to the square root of time.

We investigate horizontal submesoscale ocean mixing using long-term, highly resolved measurements of surface currents by high-frequency (HF) radar. Our submesoscale observations resolve scales of hundreds of meters to a few kilometers, and therefore fill an important gap in existing observations between fine-structure turbulence observations (millimeters to meters) and studies of the mesoscale (few tens to hundreds of kilometers). We investigate the mixing by computing the Lagrangian trajectories of thousands of ''virtual'' particles that are seeded on a uniform grid and advected by the observed two-dimensional (2D) surface velocities. Based on the calculated trajectories we calculate the single particle absolute dispersion and the relative dispersion. Our results demonstrate that both characteristics of ''diffusion-like'' mixing are violated, and hence pose a challenge to future parameterizations of ocean mixing even on such small scales.

In the next section, we describe the study region, the measurement techniques and observations, and the numerical procedure used for evaluating the submesoscale mixing environment and for identifying the barriers. In section 3, we demonstrate the existence of barriers to mixing based on the analysis of relative dispersion, and show concurrent evidence from aerial photographs. We discuss the results and conclude in section 4.

2. Methods

a. Study region

The northern terminus of the Gulf of Eilat (hereafter ''the gulf'') is a nearly rectangular, deep (~700 m), and semienclosed basin in the northeast region of the Red Sea. The gulf is bounded by desert mountains that steer the typically northerly wind along its main axis (Berman et al. 2003). Average wind speed is 4 m s^{-1} (80% of the time from the north) and net evaporation is approximately 1.6 m yr^{-1}, ranging from 1 m yr^{-1} in summer to 3–4 m yr^{-1} in winter (Ben-Sasson et al. 2009).

The surface flow can be quite complex as demonstrated in Fig. 2. The circulation in the gulf is driven by buoyancy, wind, and tides. The tide is dominated by the semidiurnal (M_2) component, which is peak forced at the Straits of Tiran (Genin and Paldor 1998; Monismith and Genin 2004; Manasrah et al. 2006). The tidally driven flux of water at the strait occupies the layer above the thermocline. In winter, when the seasonal thermocline depth exceeds 600 m, the velocity associated with this flux is significantly reduced (Monismith and Genin 2004; Berman et al. 2003). The first baroclinic Rossby radius changes seasonally, ranging from 6 (during winter) to 20 km (during summer).

The configuration and dimensions (nearly rectangular, 6 km × 10 km basin) of the northern gulf enables observation of surface currents at a very high spatial and temporal resolution using HF radar (see below), rendering the gulf a unique natural laboratory for studying submesoscale mixing processes. Two 42-MHz SeaSonde HF radar systems have been operational in the northern gulf near the city of Eilat, Israel, since August 2005. Figure 2 shows the coastline of the gulf and the locations of the two HF radars.

b. HF radar current measurements and validation

In recent years, HF radar systems for current measurements (Barrick et al. 1985; Gurgel et al. 1999b), such as the SeaSonde (Hodgins 1994) and Wellen Radar

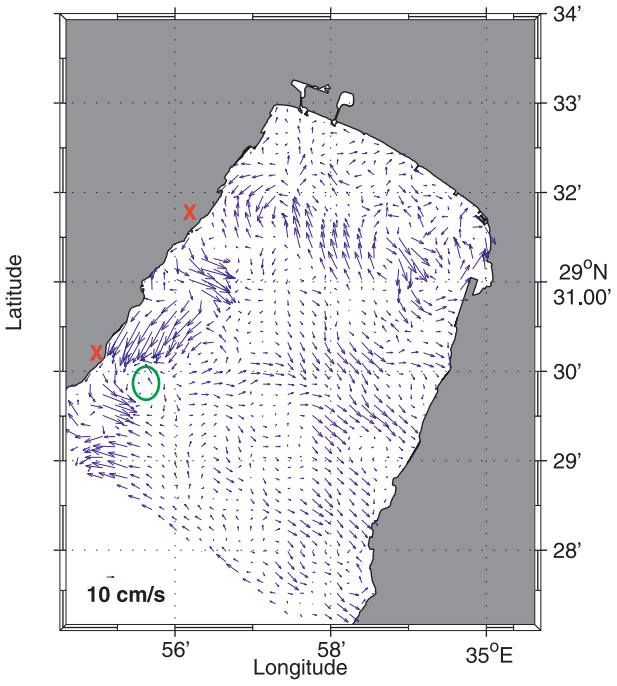

FIG. 2. The flow field at 2230 UTC 3 Feb 2006 observed by two dedicated radar stations (marked red X) after the filtering and the interpolation using OMA. The green circle represents the location of ADCP deployed during May 2006. The shape of the domain is nearly rectangular and there is only one open boundary. Although the domain is only 6 km by 10 km, there is relatively little coherence between different regions and the flow field is rather complex and variable. See scale in the bottom-left corner.

(WERA) (Gurgel et al. 1999a), have been used extensively, particularly for the study of coastal circulation. The measured currents include the Stokes drift (Monismith and Fong 2004), which results from the nonlinearity of the surface gravity waves (Mao and Heron 2008). Most of these systems operate at a frequency of around 24 MHz or lower, observing from a few tens of a kilometer up to more than hundreds of kilometers, at a resolution of a few kilometers. For the present study, we use measurements from two 42-MHz SeaSonde HF radar systems, which enable a high spatial resolution of approximately 300 m and a high temporal resolution of 30 min.

Here, we provide a brief description of the HF radar technique. Detailed descriptions of the theory of HF radar can be found in numerous articles (e.g., Gurgel et al. 1999b; Barrick et al. 1985). The radar transmits radio waves and detects the signal backscattered by the surface gravity waves, due to a Bragg resonance from those surface waves with a wavelength equal to one-half of the transmitted waves. The radial component of the phase speed of the incoming waves and outgoing waves also produce a Doppler shift in the received spectrum compared to the transmitted spectrum. If the waves are superimposed on a current, the spectral peaks are further shifted. From this additional shift, it is possible to extract the radial velocity of the current. If two radar sites measure the radial velocity of a patch of water from two different angles, it is possible to calculate the two horizontal components of the surface velocity field.

In validating the HF radar system, we compared the radar-derived velocities with those of a moored 600-kHz RD Instruments Workhorse acoustic Doppler current profiler (ADCP). The ADCP was deployed in May 2006 (see Fig. 3 for location) at approximately 26.5-m depth (variable with the tide). The ADCP recorded 1-Hz velocity measurements, which were later averaged over 5-min periods. The ADCP measurements span approximately 2–25-m depth with 0.5-m resolution (except for some bins contamined by the presence of thermistors on the mooring line). For comparison, we computed 30-min-averaged currents from the ADCP measurements at 2-m depth. The currents measured by the ADCP and by the HF radar are well correlated (correlation of around 0.8; Fig. 3). Strictly speaking, the radar measurements represent the top few tens of centimeters of the water column. However, for conditions of weak shear in the upper water column (common in the observations in Fig. 3), the HF radar measurements should be representative of currents at greater depths.

As with any remote sensing observation system, there are gaps and outliers in the HF radar data that require postprocessing, and before conducting the analysis described in section 2c, the measured currents were filtered and interpolated in order to fill spatial gaps in the observations. Several methods are available to interpolate and extrapolate the radar data, including objective mapping (Kim et al. 2007) and empirical orthogonal functions (Kaihatu et al. 1998). Another method is based on the Hodge decomposition of the velocity field (see Lekien et al. 2004), which represents the velocity field as a sum of divergence-free and irrotational modes. This method was first applied to HF radar current observations by Lipphardt et al. (2000) and we use a variant of this method called open-boundary modal analysis (OMA), which takes into account the flow through the open boundary (Lekien et al. 2004) and that can be applied to domains with arbitrary geometry. To advect the Lagrangian particles and prevent them from being accumulated on the coast, a free-slip boundary condition is applied at the coastal boundaries. An advantage of using such a method is that each mode independently satisfies the boundary condition, and therefore any combination of modes will

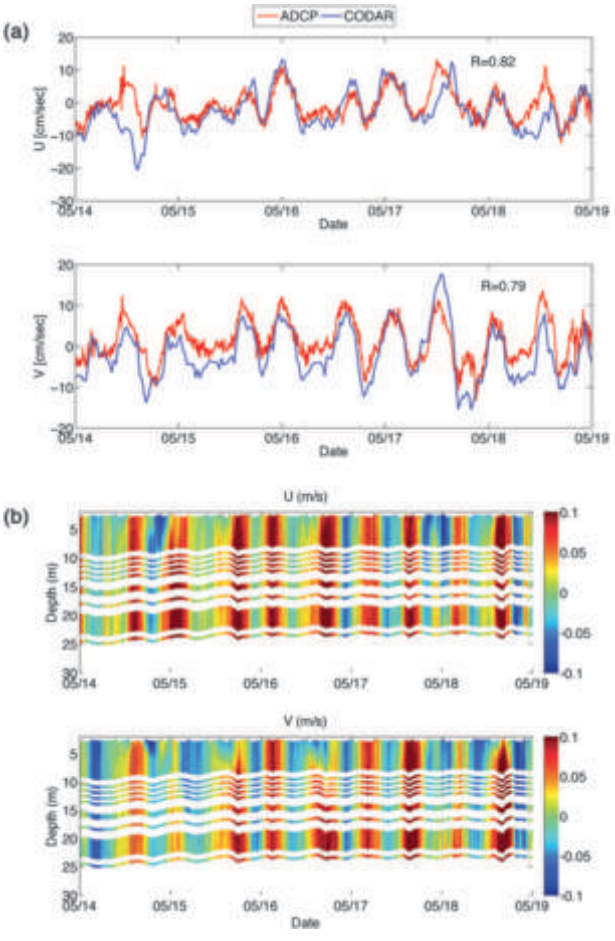

FIG. 3. (a) Comparison between the surface currents measured by the HF radar and between the surface currents measured by a 600-kHz RDI ADCP Workhorse that were conducted during May 2006 at the location marked by a green circle in Fig. 2. (b) Vertical structure of the horizontal velocity, demonstrating that most of the time the current measured by the HF radar represent the upper 10–20 m. Data gaps (white bands) for some of the bins are due to contamination from thermistors on the mooring.

satisfy the boundary conditions as well. Details on our criteria for choosing the number of modes can be found in Lekien and Gildor (2009). In summary, we use 100 divergence-free modes, 130 irrotational modes, and 40 boundary modes for reconstruction of the flow field. However, the results are not sensitive to the exact number of modes considered within a reasonable range. It is also important to note that the identified structures are also not sensitive to measurement error (Haller 2002; Lekien et al. 2005).

c. *Particle tracking and dispersion analysis*

There are numerous ways to identify regions with different mixing characteristics, including relative dispersion, finite-time Lyapunov exponents (FTLE), and finite-size Lyapunov exponents (Boffetta et al. 2001; Berloff et al. 2002; Shadden et al. 2005; Orre et al. 2006). Identification of such barriers in geophysical flows has been the focus of a number of studies in past decades (Pierrehumbert 1991; Samelson 1992; Ridderinkhof and Zimmerman 1992; Boffetta et al. 2001; Joseph and Legras 2002; d'Ovidio et al. 2004; Lekien et al. 2005; Orre et al. 2006; Lipphardt et al. 2006; Olascoaga et al. 2006; Lehahn et al. 2007). For recent reviews on the use of dynamical systems theory for oceanic applications, see Wiggins (2005) and Koshel and Prants (2006) and references therein. As mentioned above, with the exception of Lekien et al. (2005) who measured the currents at a similar resolution, these studies dealt with scales ranging from a few tens of kilometers to basin-wide phenomena. They could therefore identify fronts and filaments, but only down to a scale of a few kilometers or more. In this article we focus on flows of a few kilometers in scale and interrogate them at 300-m resolution, allowing for the identification of subkilometer flow features.

We identify barriers to mixing by calculating the relative dispersion between thousands of virtual particles advected based on the surface currents observed using HF radar. For a robust mathematical definition of a barrier, the interested reader is referred to Boffetta et al. (2001) and Shadden et al. (2005). Roughly speaking, by barrier we mean a line that separates regions with different mixing characteristics, and with little mixing across this line. Similar to previous studies (Orre et al. 2006; Haller and Yuan 2000), we find that calculations based on finite-time Lyapunov exponents yield practically identical results. A common unresolved issue in all of these methods is the treatment of particles that move out of the observed region and might recirculate back (Lekien et al. 2005). Unlike most ocean regions observed by HF radar, which include three open boundaries from which particles can enter or exit the domain (e.g., Lekien et al. 2005), in the present study the observed region has the advantage of having only one open boundary (Fig. 2).

The Lagrangian trajectories of the ''virtual'' particles are obtained by solving the following:

$$\frac{dx_k}{dt} = u_k(x_k, y_k, t)$$
$$\frac{dy_k}{dt} = v_k(x_k, y_k, t),$$

where the subscript k denotes the index of each particle ($k = 1, \ldots, N$, where N is the total number of particles), (u_k, v_k) is the velocity at the location of the particles after applying the OMA on the raw HF data, and (x_k, y_k) is the location of particle k. We assume that the

velocity of the particles is identical to that of the water (i.e., they have no inertia and they do not interact with each other). The trajectories are calculated using the forward Euler method with a time step of 6 min (integrations using different time steps and solvers show similar results). Because the temporal resolution of the measurements is 30 min and the spatial resolution is 300 m, we use linear interpolation in time and bilinear interpolation in space.

The relative dispersion (distance between initially nearby particles) at each spatial point is calculated based on the mean distance between the particle released at this point and its four nearest neighbors after a certain (finite) amount of time. Barriers, lines with a high value of relative dispersion, separate regions in which particles stay near each other. Particles that were initially on the barrier end up on both sides of the barrier, reflecting the relatively high value of relative dispersion on the barrier itself, though this does not necessarily imply divergence at the barrier.

3. Results

a. Spatial variation in mixing

Figure 4a shows the spatial distribution of the relative dispersion calculated based on 36 h of measurements starting at 0500 UTC 3 February 2006. The values of the relative dispersion between each particle and its neighbors are plotted at their initial position.

With a typical speed of 10 cm s^{-1}, and considering that 36 h includes a few tidal cycles and is a few times the turnover time of eddies in the gulf, we would expect the gulf to be well mixed after this period. Moreover, the average autocorrelation velocities over all particles is a few hours and the maximum is less than 12 h. However, the map in Fig. 4a shows that relative dispersion is far from uniform. Notably, a barrier shown by the bright color line, starting approximately at the northwestern corner of the gulf and ending at the middle of the eastern coast, can be clearly seen. The small values of the relative dispersion northeast of the dominant barrier (upper-right triangle; Fig. 4a) indicate that particles that were released within this area, tended to remain close to each other within this area. Similarly, the small values of the relative dispersion southwest of the dominant barrier indicate that particles that were released below this line also tended to stay close to each other. Particles that were released within the white area exited the domain and therefore we do not know the relative dispersion between them.

The tendency of particles which originated on one side of the barrier to stay on that side is also illustrated in Fig. 5. This figure shows the initial and final (after 36 h) areas covered by two patches of virtual ''particles'' that were released on both sides of the barrier. Clearly, particles that originated on one side of the barrier tended to stay on that side. Very few particles crossed the barrier from one side to the other.

In Fig. 6, we plot the average absolute dispersion as a function of time for the particles that were released on the two sides of the barrier. Clearly, the dependency of the absolute dispersion on time is not as expected from diffusion-like behavior. Interestingly, the dependency is different on the two sides of the barriers. Nondiffusive dispersion on similar scales was also observed in dye release experiments (Sundermeyer and Ledwell 2001). The particles originating in the northeast corner of the gulf are trapped within this region and hence their absolute dispersion (yellow line) is slower and their trajectories are more restricted than that of the particles originating southwest of the barrier (brown line), which are free to move in a larger domain. The particles released in the lower-left region reach rather fast the maximum displacements allowed by the existence of the boundaries, as can be seen from the ''saturated'' value of the brown line.

b. Aerial photographs

Because of a rare flood in this region that started on 3 February, sediments that can be seen in the aerial photo presented in the top panel of Fig. 7, were transported into the gulf. In another aerial photo taken 2 days later (bottom panel of Fig. 7, taken from a different angle), the sharp front between the muddy water and the relatively clear water was still evident. This sharp front is located approximately along the barrier identified by the calculation of the relative dispersion based on the radar measurements of the surface currents (the green rectangles in Figs. 4a and 7 mark the same location). The existence of the sharp front even 2 days after the start of the flood clearly demonstrates that mixing was not homogeneous and was relatively weak across the barrier. In the absence of a barrier, the interface between the muddy freshwater and relatively clear seawater would not have remained so sharp.

c. Temporal variations of the barriers

Mixing barriers within the gulf are highly intermittent and variable in spatial structure, and at certain times the whole region is relatively well mixed. An example for a similar barrier at a different location can be seen in Fig. 4b. In contrast, Fig. 4c is an example in which the whole region is relatively well mixed. Based on analysis of a few months of HF radar data from different seasons, similar barriers exist somewhere within the domain over 30% of the time.

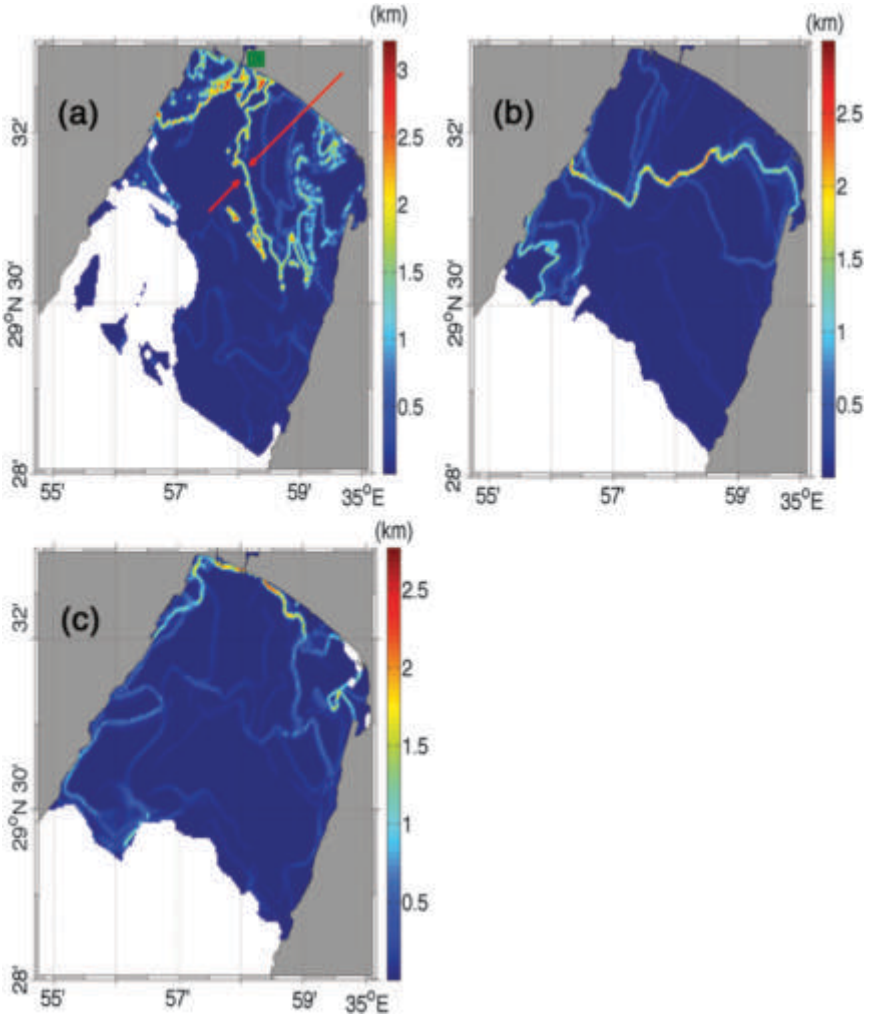

FIG. 4. Relative dispersion in the Gulf of Eilat after 36 h of particle tracking simulation using the measured HR radar surface velocities. The values of the relative dispersion between each particle and its neighbors are plotted at the initial position of this particle. (a) Starting at 0500 UTC 3 Feb 2006. The light-colored lines with higher relative dispersion values divide the domain into regions with weaker mixing. Nearby particles that were initially on the lines ended in the different regions so the distance between them grows rapidly and can be relatively large. Note the high relative dispersion line (between the red arrows) that starts in the western side of the northern coast and ends on the eastern coast. White areas are regions from which particles have moved out of the domain. The green rectangle in (a) and in Fig. 7 mark the same location. (b) Starting at 1400 UTC 3 Nov 2005. A similar barrier can be seen but at a different location. (c) Starting at 1400 UTC 15 Oct 2005. The region is relatively well mixed; no barriers crossing the interior are present.

The mechanisms behind the observed barriers are not yet clear. Sharp fronts can result from density differences (Mahadevan and Tandon 2006; Thomas et al. 2008) and may lead to a barrier because it induces a jet along the front that tends to strain the velocity field. The barrier shown in Fig. 4a might indeed result from a density difference between the muddy freshwater and the seawater. However, precipitation in general is not common in this region, and typically there is no river runoff so density differences from inflows are unlikely. Density differences caused by differential heating/cooling/evaporation might explain some of these barriers.

4. Discussion and conclusions

It has previously been demonstrated that mesoscale turbulent mixing in the ocean cannot be well represented by eddy diffusivity because the velocity distribution is

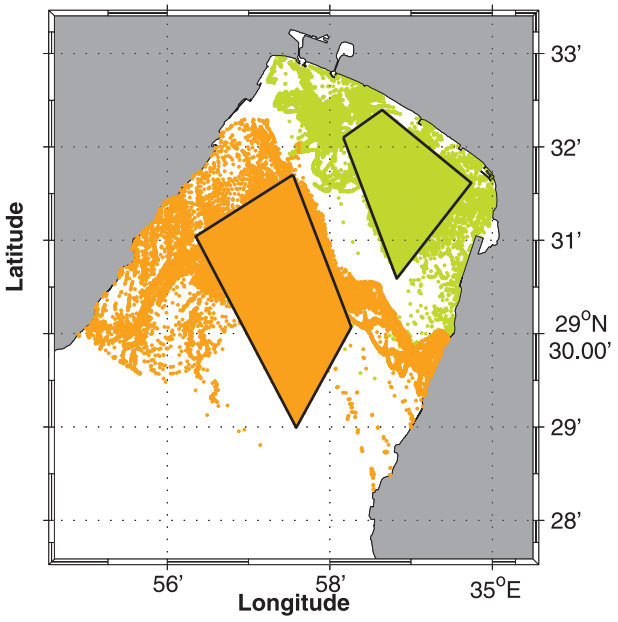

FIG. 5. The locations of particles originating from both sides of the barrier after 36 h for the simulation starting at 1400 UTC 3 Feb 2006. Particles marked by yellow dots were released within the black trapezoid in the upper-right side (northeast) of the barrier while the particles marked by brown dots were released in the lower-left side (southwest side of the barrier). Particles originating on one side of the barrier tend to stay on that side, and there is almost no mixing between the two sides of the barrier.

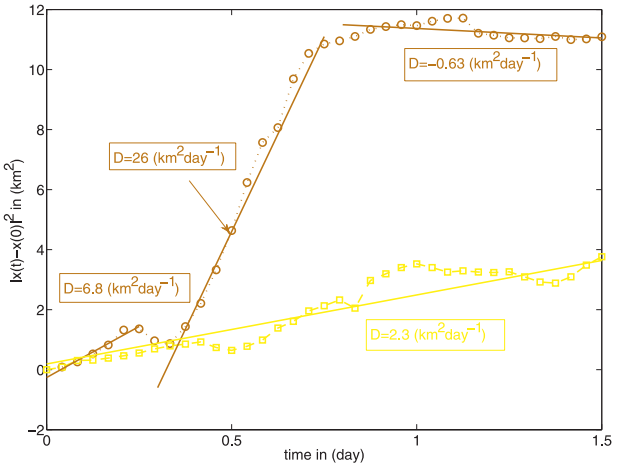

FIG. 6. Average absolute dispersion as a function of time for the particles shown in Fig. 3 (the results are not sensitive to specific location of the trapezoid in Fig. 6). (brown) For the particles originating on the southwest side of the barrier. (yellow) For the particles originating northeast of the barrier. The time dependence of the absolute dispersion is different on the two sides of the barrier. Unlike diffusion-like mixing, the absolute dispersion does not grow as the square root of the time.

non-Gaussian (Bracco et al. 2003) and because barriers to mixing exist on these scale (d'Ovidio et al. 2004; Olascoaga et al. 2006; Lehahn et al. 2007; Berloff et al. 2002). For the atmosphere, it was demonstrated even earlier (Pierrehumbert 1991 and references therein). However, it was generally assumed that on scales smaller than the internal Rossby radius, the relative dispersion is isotropic (LaCasce 2008).

Here we analyzed submesoscale ocean mixing using high-resolution measurements of surface currents. The flow field in the observed area is quite energetic, complex, and variable, and one would expect that over a time scale of a day, this small region would be well mixed. The autocorrelation of the flow field is less than 12 h. Yet, our results suggest that mixing is far from uniform even on such a relatively small spatial scale of a few kilometers. Rather, our results show many clear instances of barriers to mixing and transport (see also Lekien et al. 2005), based on calculations of the relative dispersion derived from observed current data and also observed in aerial photographs. Such barriers, when present, could act to trap passive scalars such as larvae or pollutants. Interestingly, a recent study on fish recruitment in this region reports a clear distinction in both the age of recruitment and the chemical signature of the otolith between fish that settle on the northern and eastern boundaries of this region and those settled on the western side (Ben-Tzvi et al. 2008). It seems quite possible that the complex mixing behavior observed here may be a common feature of submesoscale surface currents in the ocean. Therefore, these results challenge the common usage of eddy diffusivity to represent subgrid processes in ocean models, even when the grid size is as small as a few kilometers.

A primary limitation of our analysis is the negligence of vertical velocity, which is known to be important in submesoscale dynamics (Mahadevan and Tandon 2006; Thomas et al. 2008). Yet, even in the presence of vertical motion, these barriers are relevant for floating biological material and pollutants (e.g., oil), which tend to stay near the sea surface.

The barriers and mixing characteristics presented in this study have been identified from the measured currents and in one case have been verified by aerial photographs. The mechanism behind the barriers is still unknown and remains an open research question. Unfortunately, we lack information of the spatial variability of surface forcing such as wind stress and buoyancy fluxes. We note, though, that such barriers have been identified during different seasons.

Because our analysis shows that barriers can persist for more than a day, they can be taken into account in short-term prediction in cases of oil spills or search-and-rescue missions (e.g., Lekien et al. 2005). By analyzing the observed currents measured by HF radar in real

FIG. 7. Barrier to mixing as seen by aerial photographs showing that the sediments do not mix beyond the barrier that was calculated from the currents observed by the HF radar. (a) Taken from the northwestern corner of the gulf toward southeast on 3 Feb 2006. (b) Taken from inside the gulf facing northwest on 5 Feb, two days after the flood. The green rectangle in Fig. 4a and in this figure mark the same location. (Photos by Dubi Tal, Albatross Photography.)

time, it is possible to identify the barriers and regions with different mixing characteristics soon after these barriers start to emerge, and consider their existence when trying to predict trajectories of passive scalars on time scales of tens of hours.

Acknowledgments. This research was supported by The Israel Science Foundation (Grant 781/04) and by NATO SfP982220. HG is the Incumbent of the Rowland and Sylvia Schaefer Career Development Chair and is supported by a research grant from the Estate of Sanford Kaplan. We thank Amatzia Genin, Roi Holzman, and Jeff Koseff for their help with the ADCP deployment. The Port in Eilat gave us permission to install one of the sites in its area. Airspan provided us with the wireless communication between the radar sites. We thank the management and the staff of the Inter-University Institute for Marine Sciences of Eilat (IUI) for their cooperation and help.

REFERENCES

Barrick, D. E., B. J. Lipa, and R. D. Crissman, 1985: Mapping surface currents with codar. *Sea Technol.,* **26** (10), 43–47.

Ben-Sasson, M., S. Brenner, and N. Paldor, 2009: Estimating air–sea heat fluxes in semienclosed basins: The case of the Gulf of Elat (Aqaba). *J. Phys. Oceanogr.,* **39,** 185–202.

Ben-Tzvi, O., A. Abelson, S. Gaines, M. El-Zibdah, M. Sheehy, G. Paradis, and M. Kiflawi, 2008: Tracking recruitment pathways of Chromis viridis in the Gulf of Aqaba using otolith chemistry. *Mar. Ecol. Prog. Ser.,* **73** (4), 229–238.

Berloff, P. S., J. C. McWilliams, and A. Bracco, 2002: Material transport in oceanic gyres. Part I: Phenomenology. *J. Phys. Oceanogr.,* **32,** 764–796.

Berman, T., N. Paldor, and S. Brenner, 2003: The seasonality of tidal circulation in the Gulf of Elat. *Isr. J. Earth Sci.,* **52,** 11–19.

Boffetta, G., G. Lacorata, G. Radaelli, and A. Vulpiani, 2001: Detecting barriers to transport: A review of different techniques. *Physica D,* **159** (1–2), 58–70.

Bracco, A., E. Chassignet, Z. Garraffo, and A. Provenzale, 2003: Lagrangian velocity distributions in a high-resolution numerical simulation of the North Atlantic. *J. Atmos. Oceanic Technol.,* **20,** 1212–1220.

Capet, X., J. C. Mcwilliams, M. J. Mokemaker, and A. F. Shchepetkin, 2008: Mesoscale to submesoscale transition in the California Current system. Part I: Flow structure, eddy flux, and observational tests. *J. Phys. Oceanogr.,* **38,** 29–43.

d'Ovidio, F., V. Fernandez, E. Hernandez-Garcia, and C. Lopez, 2004: Mixing structure in the Mediterranean Sea from finite-size Lyapunov exponents. *Geophys. Res. Lett.,* **31,** L17203, doi:10.1029/2004GL020328.

Garcia-Olivares, A., J. Isern-Fontanet, and E. Garcia-Ladona, 2007: Dispersion of passive tracers and finite-scale Lyapunov exponents in the Western Mediterranean Sea. *Deep-Sea Res.,* **54** (2), 253–268, doi:10.1016/j.dsr.2006.10.009.

Genin, A., and N. Paldor, 1998: Changes in the circulation and current spectrum near the tip of the narrow, seasonally mixed Gulf of Elat. *Isr. J. Earth Sci.,* **47,** 87–92.

Gurgel, K. W., G. Antonischki, H. H. Essen, and T. Schlick, 1999a: Wellen radar (WERA): A new ground-wave HF radar for ocean remote sensing. *Coastal Eng.,* **37** (3–4), 219–234.

——, H. H. Essen, and S. P. Kingsley, 1999b: High-frequency radars: Physical limitations and recent developments. *Coastal Eng.,* **37** (3–4), 201–218.

Haller, G., 2002: Lagrangian coherent structures from approximate velocity data. *Phys. Fluids,* **14** (6), 1851–1861.

——, and G. Yuan, 2000: Lagrangian coherent structures and mixing in two-dimensional turbulence. *Physica D,* **147,** 352–370.

Hodgins, D., 1994: Remote-sensing of ocean surface currents with the SeaSonde HF radar. *Spill Sci. Technol. Bull.,* **1** (2), 109–129.

Joseph, B., and B. Legras, 2002: Relation between kinematic boundaries, stirring, and barriers for the Antarctic polar vortex. *J. Atmos. Sci.,* **59,** 1198–1212.

Kaihatu, J., R. Handler, G. Marmorino, and L. Shay, 1998: Empirical orthogonal function analysis of ocean surface currents using complex and real-vector methods. *J. Atmos. Oceanic Technol.,* **15,** 927–941.

Kim, S. Y., E. Terrill, and B. Cornuelle, 2007: Objectively mapping HF radar-derived surface current data using measured and idealized data covariance matrices. *J. Geophys. Res.,* **112,** C06021, doi:10.1029/2006JC003756.

Koshel, K. V., and S. V. Prants, 2006: Chaotic advection in the ocean. *Phys.-Uspekhi,* **49** (11), 1151–1178, doi:10.1070/PU2006v049nl1ABEH006066.

LaCasce, J., 2008: Statistics from Lagrangian observations. *Prog. Oceanogr.,* **77,** 1–29, doi:10.1016/j.pocean.2008.02.002.

——, and C. Ohlmann, 2003: Relative dispersion at the surface of the Gulf of Mexico. *J. Mar. Res.,* **61** (3), 285–312.

Lehahn, Y., F. d'Ovidio, M. Levy, and E. Heifetz, 2007: Stirring of the northeast Atlantic spring bloom: A Lagrangian analysis based on multisatellite data. *J. Geophys. Res.,* **112,** C08005, doi:10.1029/2006JC03927.

Lekien, F., and H. Gildor, 2009: Computation and approximation of the length scales of harmonic modes with application to the mapping of surface currents in the Gulf of Eilat. *J. Geophys. Res.,* **114,** C06024, doi:doi:10.1029/2008JC004742.

——, C. Coulliette, R. Bank, and J. Marsden, 2004: Open-boundary modal analysis: Interpolation, extrapolation, and filtering. *J. Geophys. Res.,* **109,** C12004, doi:10.1029/2004JC002323.

——, ——, A. J. Mariano, E. H. Ryan, L. K. Shay, G. Haller, and J. Marsden, 2005: Pollution release tied to invariant manifolds: A case study for the coast of Florida. *Physica D,* **210** (1–2), 1–20.

Lipphardt, B. L., A. D. Kirwan, C. E. Grosch, J. K. Lewis, and J. D. Paduan, 2000: Blending HF radar and model velocities in Monterey Bay through normal mode analysis. *J. Geophys. Res.,* **105** (C2), 3425–3450.

——, D. Small, A. D. Kirwan, S. Wiggins, K. Ide, C. E. Grosch, and J. D. Paduan, 2006: Synoptic Lagrangian maps: Application to surface transport in Monterey Bay. *J. Mar. Res.,* **64** (2), 221–247.

Mahadevan, A., and A. Tandon, 2006: An analysis of mechanisms for submesoscale vertical motion at ocean fronts. *Ocean Modell.,* **14** (3–4), 241–256.

Manasrah, R. S., F. A. Al-Horani, M. Y. Rasheed, S. A. Al-Rousan, and M. A. Khalaf, 2006: Patterns of summer vertical and horizontal currents in coastal waters of the northern Gulf of Aqaba, Red Sea. *Estuarine Coastal Shelf Sci.,* **69** (3–4), 567–579.

Mao, Y., and M. L. Heron, 2008: The influence of fetch on the response of surface currents to wind studied by HF ocean surface radar. *J. Phys. Oceanogr.,* **38,** 1107–1121.

Monismith, S. G., and D. A. Fong, 2004: A note on the potential transport of scalars and organisms by surface waves. *Limnol. Oceanogr.,* **49,** 1214–1217.

——, and A. Genin, 2004: Tides and sea level in the Gulf of Aqaba (Eilat). *J. Geophys. Res.,* **109,** C04015, doi:10.1029/2003JC002069.

Olascoaga, M. J., I. I. Rypina, M. G. Brown, F. J. Beron-Vera, H. Kocak, L. E. Brand, G. R. Halliwell, and L. K. Shay, 2006: Persistent transport barrier on the west Florida shelf. *Geophys. Res. Lett.,* **33,** L22603, doi:10.1029/2006GL027800.

Orre, S., B. Gjevik, and J. H. Lacasce, 2006: Characterizing chaotic dispersion in a coastal tidal model. *Cont. Shelf Res.,* **26** (12–13), 1360–1374.

Pierrehumbert, R., 1991: Chaotic mixing of tracer and vorticity by modulated traveling Rossby waves. *Geophys. Astrophys. Fluid Dyn.,* **58** (1–4), 285–319.

Ridderinkhof, H., and J. Zimmerman, 1992: Chaotic stirring in a tidal system. *Science,* **258** (5085), 1107–1111.

Samelson, R., 1992: Fluid exchange across a meandering jet. *J. Phys. Oceanogr.,* **22,** 431–440.

Shadden, S. C., F. Lekien, and J. E. Marsden, 2005: Definition and properties of Lagrangian coherent structures from finite-time Lyapunov exponents in two-dimensional aperiodic flows. *Physica D,* **212** (3–4), 271–304.

Sundermeyer, M. A., and J. R. Ledwell, 2001: Lateral dispersion over the continental shelf: Analysis of dye release experiments. *J. Geophys. Res.,* **106** (C5), 9603–9621.

Thomas, L. N., A. Tandon, and A. Mahadevan, 2008: Submesoscale processes and dynamics. *Eddy Resolving Ocean Modeling,* M. W. Hecht and H. Hasumi, Eds., Amer. Geophys. Union, 17–38.

Van Haren, H., L. S. Laurent, and D. Marshall, 2004: Small and mesoscale processes and their impact on the large scale: An introduction. *Deep-Sea Res.,* **51** (25–26), 2883–2887.

Waugh, D. W., E. R. Abraham, and M. M. Bowen, 2006: Spatial variations of stirring in the surface ocean: A case study of the Tasman Sea. *J. Phys. Oceanogr.,* **36,** 526–542.

Wiggins, S., 2005: The dynamical systems approach to Lagrangian transport in oceanic flows. *Annu. Rev. Fluid Mech.,* **37,** 295–328, doi:10.1146/annurev.fluid.37.061903.175815.

Williams, R., and M. Follows, 2003: Physical transport of nutrients and the maintenance of biological production. *Ocean Biogeochemistry,* M. J. R. Fasham, Ed., Springer-Verlag, 19–49.